Supplementary Material

Proteins and Lipids

Proteins were expressed, purified, and reconstituted into vesicles as described previously (S1). The specific proteins include: the v-SNARE protein mouse synaptobrevin-2, here referred to as syb; and the full-length binary t-SNARE complex composed of rat syntaxin 1A (syx) and mouse SNAP25B. All phospholipids were purchased from Avanti Polar Lipids (Alabaster, AL). We use synthetic 1-palmitoyl,2-oleoyl phosphatidylcholine (POPC), 1,2-dioleoyl phosphatidylserine (DOPS) and 1,2-dioleoyl phosphatidylethanolamine (DOPE). The lipid probes and content probes used to label v-SNARE vesicles are from Molecular Probes (Eugene, OR), including: *N*-(tetramethylrhodamine)-1,2-diheptadecanoyl phosphatidylethanolamine (TRITC-DHPE), octadecyl rhodamine B chloride (R18), *N*-(Texas Red)-1,2-dihexadecanoyl-*sn*-glycero-3-phosphoethanolamine triethylammonium salt (Texas Red-DHPE), and calcein, a polyanionic derivative of fluorescein (high purity, Molecular Probes).

Doubly-labeled v-SNARE vesicles were reconstituted by co-micellization followed by rapid dilution and then separated from detergent, unincorporated protein, lipids, and calcein by size exclusion columns made with the resin Sepharose CL4B (Amersham Biosciences, UK). The protein content was ~80 v-SNARE copies/vesicle. All v-SNARE vesicles were reconstituted with 15% DOPS. For those without DOPE, the total percentage of POPC plus lipid probes was 85%. For those with 30% DOPE, the total percentage of POPC plus lipid probes was 55%. For those with 60% DOPE, the total percentage of POPC plus lipid probes was 25%. R18 and Texas Red-DHPE were used at 5% to obtain strong dequenching/polarization enhancement of fluorescence intensity after fusion (S1). TRITC-DHPE at only 1% produced a similar enhancement.

To label the v-SNARE vesicle content, 50 mM calcein was included in both elution buffer and dialysis buffer during the reconstitution procedures, which was carried out at pH 7. We qualitatively confirmed the pH of the small volumes of buffer using pH paper (Micro Essential Laboratory, Brooklyn, NY). Calcein has a net charge of –4 at pH 7.4, which helps prevent insertion into the vesicle bilayer and leaking through the bilayer. In other work, the half-time of calcein retention within protein-free liposomes was measured to be on the order of weeks (S2). Our v-SNARE vesicles do not leak calcein content for at least two days when stored at 4°C after preparation. The release of calcein from v-SNARE vesicles upon fusion is marked by a sharp increase of calcein fluorescence intensity due to dequenching. Measurements of the degree of calcein self-quenching vs concentration are described below.

Fluorescence Microscopy and Data Analysis

A modified commercial wide-field microscope (Eclipse TE2000-U, Nikon, Melville, NY) enables excitation of fluorophores at the glass/water interface by "through the objective" total internal reflection (TIR) (S3). The evanescent wave illuminates a ~100-nm high cylinder including the lipid bilayer. A 60×, 1.45 numerical aperture, oil-immersion objective (Olympus,

Melville, NY) combined with the Nikon tube lens made the effective magnification of the microscope 100x. Lasers at 488 nm (Ar^+, Melles Griot), 514 nm (Ar^+, Melles Griot) and 561 nm (Crystal Laser) were used to excite calcein, TRITC-DHPE, and R18/Texas Red-DHPE, respectively. To simultaneously excite the content dye (calcein) and lipid dye (R18 or Texas Red DHPE), a beam combiner z488bcm (Chroma, Rockingham, VT) was used to align the 488 nm and 561 nm lasers on top of each other. A dual band dichroic mirror z488/561rpc (Chroma) was used to reflect both laser lines and pass the fluorescence emissions from both dyes. The combined laser beams were expanded together and focused onto the back focal plane of the objective with an achromatic lens. A circular area of diameter ~14 μm was illuminated with 5−20 μW total intensity at 488 nm and 5−15 μW total intensity at 561 nm. The fluorescence from the two dyes was collected by the objective, then spectrally separated by a long-pass filter (560-dclp, Chroma) and imaged onto separate halves of the ccd chip. Emission filters HQ525/50M and HQ675/50M (Chroma) were included in the short and long wavelength paths, respectively.

In one-color experiments using TRITC or Texas Red labels (Fig. S1a and c), hemifusion (outer leaflet mixing) is marked by a sharp increase due to dequenching of the labels as the outer leaflet mixes with lipids in the planar bilayer and to enhanced excitation and emission detection as the rhodamine labels flatten onto the planar bilayer (S4). Referring to Fig. S1-a, time $t = 0$ is taken as the onset of firm vesicle docking. The decay of intensity up to $t \sim 1.12$ s, is due to diffusion of part of the TRITC-DHPE out of the circle of integration. At $t = 1.12$ s, a second dequenching event occurs, followed by outward diffusion of all remaining labels. We attribute the second burst of fluorescence to the fusion of inner-leaflet lipids (core fusion). Visual inspection of the movie confirms this interpretation. When TRITC-DHPE is used at 1%, some hemifusion events showed only a change in slope of intensity vs time, not a clear second intensity burst. In those cases, we could still see the residual core by eye.

A two-color experiment to simultaneously monitor lipid mixing and content release using the standard content label calcein requires a lipid marker that emits at longer wavelength than TRITC to minimize spectral overlap. We chose the standard lipid marker R18 for its red-shifted spectrum and commercial availability. Figure S1b shows a typical one-color hemifusion event using 5% R18 as the lipid marker in a movie taken at 40 ms/frame. At this concentration, dequenching at t_{hemi} is clear, but the second burst of intensity due to core fusion is observed only weakly if at all. In this particular example, we are able to measure t_{core} only by careful visual inspection of the movie. As explained in the primary text, fast flip-flop of the R18 labels on a ~200 ms timescale greatly diminishes the amplitude of the second burst. Dequenching of the calcein content signal proves to be a much more sensitive marker of t_{core}.

We also tried the lipid label Texas-Red-DHPE, whose spectrum is compatible with calcein. An example of a hemifusion intensity trace using 5% Texas Red-DHPE is shown in Fig. S1c. Dequenching is very strong, and second bursts marking t_{core} are readily observed in most cases for which we can see the persistent core by eye. The Texas Red labels proved useful in demonstrating that the calcein content intensity burst always coincides in time with core lipid fusion. However, in Table S1 we show evidence that the Texas Red label, which is larger than TRITC or rhodamine, decreases the fraction of hemifusion events. Therefore, most of this study

used R18 as the lipid marker.

Self-quenching Properties of Calcein

Calcein is strongly self-quenched at the 50 mM concentration in the v-SNARE vesicles. The calcein *relative* fluorescence quantum yield, ϕ_{rel}, vs concentration is necessary for quantitative modeling of the decay in calcein intensity vs time after dequenching. The calcein fluorescence lifetime at low concentration is 4 ns, suggesting a fluorescence quantum yield near one. For convenience, we define ϕ_{rel} to be 1 for calcein in dilute solution. At self-quenching concentrations, ϕ_{rel} gives the relative fluorescence intensity per molecule. Initially, we attempted to measure ϕ_{rel} in a standard fluorimeter with a 1cm long cuvette (Fig. 4b). The fluorescence intensity per molecule decreased more than 3 orders of magnitude as we increased the calcein concentration from 100 μM to 1 mM, roughly consistent with the findings of Bowen et al (S5). However, even for a 1 mM calcein solution, essentially no excitation light reaches the center of the cuvette, the region from which fluorescence is collected (base 10 molar absorptivity 77,000 $M^{-1}cm^{-1}$ at λ_{ex} = 494 nm, PH=9, Molecular Probes). This "inner filter effect" (S6) causes severe overestimation of the self-quenching factor by 2-3 orders of magnitude.

To obtain an extremely thin excitation volume, we utilized the evanescent wave generated by the 488-nm laser beam to excite calcein in neutral buffer solution in a standard sample cell. Calcein fluorescence was collected by the objective and detected on the ccd camera through a 500-550 nm bandpass filter as usual. The evanescent wave penetrates only 100-200 nm into the calcein solution. Even for 75 mM calcein solution, 77% of the excitation light can penetrate a 200 nm thick sample, and all the emitted light escapes the solution. As shown in Fig. 3b, results were the same using hydrophilic glass as the surface or using hydrophilic glass covered by a supported lipid bilayer (2% DOPS, 98% POPC). Evidently the highly negatively charged calcein dye at neutral pH (approximately –4 charge) does not stick to the clean, negatively charged glass surface, i.e., the contribution from calcein adhered to the surface is negligible. We confirmed the TIRF results with a confocal microscope using epi illumination with the objective focused just above the coverslip (data not shown). The observation depth is ~1-2 μm; 98.2% of the excitation light penetrates 1 μm into 1 mM calcein solution. The results for ϕ_{rel} are consistent with the TIRF measurements.

FRET from Calcein to R18 Prior to Core Fusion

The evidence for fluorescence resonant energy transfer (FRET) from calcein to R18 is fourfold. First, the calcein emission spectrum significantly overlaps the R18 absorption spectrum. We have measured these spectra to estimate the calcein/R18 Förster radius to be $R_0 \sim 5$ nm; the exact number depends on the fluorescence quantum yield, which varies with concentration. A typical 50-nm diameter vesicle contains ~1000 calcein molecules (at 50 mM) and ~1300 R18 labels (at 5% labeling fraction). If calcein is uniformly distributed inside the vesicle, simple geometry shows that in a 50-nm diameter vesicle, ~50% of the calcein molecules lie within R_0 of an inner-leaflet R18 label. At 50 mM, the mean distance between calcein molecules is only ~3 nm. The FRET efficiency might be further enhanced by excitation

migration from the center of the vesicle to its periphery via homo-FRET among the calcein molecules. Prior to release of any inner-leaflet labels, the FRET efficiency of calcein to R18 should be quite high. This qualitatively agrees with the slow, factor-of-two increase in calcein intensity vs time in Type 3 events. Furthermore, outer-leaflet R18 labels lie more than 5 nm from calcein, so the FRET efficiency between calcein and outer-leaflet labels should be small. Second, we have used bulk fluorimetry on protein-free vesicles containing 50 mM calcein and 5% R18 labels to demonstrate that FRET in fact occurs (Fig. S4). Third, careful examination of the calcein signal in Type 2 events (productive hemifusion) shows that it also typically increases in the interval t_{core} between hemifusion and core fusion, albeit by a smaller percentage than observed in Type 3 events. The values of t_{core}, as measured by the calcein dequenching event, vary widely. With 60% DOPE in the v-SNARE vesicle, the range of t_{core} is 0.015–4.1 s. Almost all of the events with t_{core} greater than 200 ms show increasing calcein signal during t_{core}. This behavior is again consistent with relief of FRET quenching as R18 flip-flop occurs, but there is less time for flip-flop to occur than in Type 3 events.

Tests for kinetic effects of laser intensity, content label, and lipid label

Brunger, Chu and co-workers (S5) found that SNARE-dependent fusion of proteoliposomes onto a planar lipid bilayer on a 10-s time scale was driven primarily by the temperature rise due to laser heating of the self-quenched calcein content at 200 mM. Our v-SNARE vesicles are prepared with calcein content at 50 mM. To test for possible heating effects, we compared ensemble fusion kinetics at two different 488 nm laser intensities. Using v-SNARE vesicles with 60% DOPE and labeled with 5% R18 and 50 mM calcein, we obtained 5 ms, two-channel movies using either the usual 5.6 μW at 488 nm or 19.6 μW at 488 nm, 3.5 times larger. Histograms of the distribution of times between outer-leaflet lipid diffusion and content release ($t_{calcein}$) for single fusion events for the high and low laser intensities look nearly identical (Fig. S5), indicating that in our system laser heating is not a major driving force for fusion. The difference between the two studies may arise from our fourfold smaller calcein concentration; in addition, fusion is so fast in our assay that the vesicle may not have time to warm significantly prior to the fusion event.

We also tested for possible effects of illumination by two lasers vs one and of different lipid labels on the fusion kinetics. We obtained one-channel, 40-ms/frame one-color movies for v-SNARE vesicles labeled with 1% TRITC-DHPE, or 5% R18, or 5% TexasRed-DHPE, with and without 50 mM calcein, and with and without the 488 nm laser on. Histograms of t_{fus} made for each combination look very similar (data not shown), indicating that the full fusion kinetics are not affected by these variables. The percentage of vesicles that fuse through a hemifusion intermediate also appears to be unaffected by content labeling or excitation by the 488 nm laser (Table S1). However, the percentage of hemifusion events does depend on the choice of lipid label. We observed fewer hemifusion events for 5% Texas Red-DHPE labeling as compared with 1% TRITC-DHPE. Texas Red is a substantially larger molecule than Rhodamine and required a higher percentage to produce a dequenching rise in signal. It may facilitate core fusion in much the same way as “positively curved” species such as lysolipids (S7). For vesicles labeled only with R18, flip-flop prevents observation of very many hemifusion events.

Quantitative comparison of productive hemifusion events using the single TRITC-DHPE label vs the dual R18/calcein labels suggests that the labels are non-perturbative. The shortest delay time between hemifusion and core fusion that we can detect in one-channel, 40 ms/frame movies of TRITC-DHPE labeled vesicles is ~160 ms. If in the two-channel movies with 60% DOPE and R18/calcein labeling we only count those productive hemifusion events in which $t_{core} > 160$ ms, then the percentage of productive hemifusion events would be reduced from 35% (Table 1) to 14%, in good agreement with the new TRITC-DHPE results in Table S1 and with the earlier hemifusion study (S4). Furthermore, the histogram of t_{core} for the same subset of events ($t_{core} \geq 160$ ms) in the two-channel movies with R18/calcein labeling is very similar to the histogram of t_{core} in one-channel movies for TRITC-DHPE labeled vesicles (Fig. S6). This suggests that the kinetics of productive hemifusion are very similar for the 1% TRITC-DHPE and 5% R18/50 mM calcein labeling schemes.

2D and 3D diffusion models

Our goal is to calculate the decay in time of the integrated calcein fluorescence intensity $F(t)$ within a 1.2 μm radius circle for three-dimensional (3D) vs two-dimensional (2D) diffusion after content release. The time-dependent integrated intensity is an integral over a cylindrical observation volume of radius $R = 1.2$ μm and height h. We use cylindrical coordinates (ρ,z) to match the symmetry of the problem:

$$F(t) = A \int_0^R 2\pi\rho \, d\rho \int_0^h C(\rho,z,t) \, \phi_{rel}(\rho,z,t) \, I_{laser}(z) dz \qquad \text{(S1)}$$

Here ρ is the distance from the symmetry axis (z-axis), and $z = 0$ is defined by the glass/bilayer interface. The calcein concentration $C(\rho,z,t)$ is determined by the 2D or 3D diffusion equation. The calcein relative fluorescence quantum yield ϕ_{rel} depends strongly on concentration due to the self-quenching described in the method section, and thus on both spatial coordinates and time. The evanescent field intensity I_{laser} depends on z according to $I(z) = I_0 \exp(-z / z_0)$, with $z_0 \approx 100$ nm for our objective (numerical aperture NA = 1.45). The time-independent proportionality constant A takes account of light collection efficiency, filter factors, detector quantum yield, etc.

In the 2D case, we assume that the total number of calcein molecules, $N_0 = C_0 V_{ves}$, is released instantaneously from the origin and expands in an effectively two-dimensional thin water layer between the planar bilayer and the glass surface layer of height h = 1-2 nm. Here C_0 is the pre-fusion calcein concentration within the intact vesicle of volume V_{ves}. The analytical solution to the time-dependent, 2D diffusion equation is standard:

$$C(\rho,t) = \frac{C_0 V_{ves}}{4\pi h D t} \times e^{-\rho^2/4Dt} \qquad \text{(S2)}$$

As a first approximation, we tried the values $C_0 = 50$ mM and $D = 200$ μm^2-s^{-1} for calcein. This solution-phase value of the calcein diffusion coefficient is almost surely an overestimate for diffusion in the thin volume of interest. In the 2D case, the laser intensity is assumed constant

over the observation thickness h.

We approximated Eq. S1 numerically as a sum over a circle of 100-nm radius plus 11 annular regions in the xy plane, with successive annular radii increasing by 100 nm. The integration over z brings a factor of h that cancels the h in the denominator of Eq. S2.

We evaluated $F_{2D}(t)$ from $t = 0$ to 55.5 ms in 50 μs time intervals. To compare the calculated intensity traces with the experimental traces $I_{1.2\mu m}(t)$, we averaged the calculated values over 1 ms time intervals to match the camera exposure time. Because the onset of calcein release can start anytime within a 1 ms frame, we generated 10 model intensity traces with the onset of fusion shifted within the first frame in 0.1 ms increments. This phase shift primarily affects the first two data points above the baseline, not the time scale of the decay. We selected the phase shift that produces the best match to the data.

With $C_0 = 50$ mM and $D = 200$ μm^2-s^{-1}, the decay of $F_{2D}(t)$ is much slower than the experimental decay (Fig. 4a). Calcein deposited between the bilayer and glass almost surely diffuses more slowly, which would make the agreement even worse. Only for D ~800 μm^2-s^{-1}, some four times larger than the solution phase diffusion coefficient, does the agreement become reasonably good. The shape of $\phi_{rel}(\rho,t)$ depends on the initial calcein concentration within the vesicle. When we make vesicles with nominal 50 mM content, individual vesicles may leak to a variable extent before the fusion experiment, so 50 mM is really an upper limit . Therefore we varied C_0 over the range 10-50 mM. At lower concentrations, the docking intensity is larger relative to the peak, but the decay is always determined by the diffusion coefficient and is far too slow. If the content leaked slowly out of the vesicle into the 2D space, this would only slow the intensity decay further. In summary, it appears impossible to quantitatively model the data using two-dimensional diffusion.

Therefore we explored a 3D model of calcein diffusion, in which we assume the vesicle bursts and suddenly releases all its content at the origin at $t = 0$, after which calcein diffuses freely in a three-dimensional half-space (above the plane of the bilayer) with $D = 200$ μm^2-s^{-1}. The analytical equation for 3D free diffusion from a point source into an infinite half-space lying above the plane of the bilayer (S6) is:

$$C(\rho, z, t) = \frac{2C_0 V_{ves}}{(4\pi D t)^{3/2}} e^{-(\rho^2+z^2)/4Dt} \qquad \text{(S3)}$$

A factor of two is included because calcein is confined into a half sphere. In the 3D model we again evaluate Eq. S1 numerically using cylindrical coordinates (ρ,z). For each value of z, the lateral distribution is a Gaussian as in the 2D case, so the numerical integration over ρ was carried out in analogous fashion. The fluorescence intensity from each horizontal plane properly includes the ρ-dependent value of ϕ_{rel} and the laser intensity factor $I_{laser}(z)$. Again, due to the unknown phase shift between the onset of fusion and the camera frames, 10 model intensity decay traces were generated for comparison with experiment.

Comparison of experimental fusion traces with the 2D and 3D model intensity decay traces with the closest shape (Fig. 4a) revealed that, the 3D model matches the data very well, while

the 2D model decays much slower than real data. We believe that, contrary to our expectations, when the v-SNARE vesicle fuses with the planar lipid bilayer, the calcein is released into the space above bilayer.

Diffusion-limited response time of lipid-based probes of fusion

The R18 dequenching/re-orientation events characterized by $t_{R18\ rise}$ usually occur more slowly than the 5 ms camera frame time (Fig. S8). We may well be approaching a fundamental timing limit on the measurement of fast fusion events using dequenching of lipid-based labels. Assuming the kinetics of rhodamine dimer dissociation is faster than the low-ms time scale of interest, the limit is probably set by the time scale of diffusion of labels within the vesicle bilayer to find the small area or seam where lipids from the vesicle and planar bilayer exchange.

The closely related model problem of diffusion to capture on the surface of a sphere has been solved (S8, S9). The solution provides a simple formula for the mean time at which molecules of diffusion coefficient D, which uniformly coat the surface of a sphere of radius R at $t = 0$, find a "target" small circle of radius b subtending the cone angle $\theta_c = \tan^{-1}(b/R)$ as measured from the center of the sphere. The result takes the form $<\tau_{capture}> = (R^2/D)f(\theta_c)$. The function $f(\theta_c)$ contains terms in $(1 + \cos\theta_c)$ and $ln(1 - \cos\theta_c)$, both of which vary slowly with b for fixed R when b/R is small; see Eqs. 7a and 7b of Ref. S9. As a rough time scale, we obtain $<\tau_{capture}> = 2.0$ ms using the sensible estimates $D = 2\ \mu m^2\text{-}s^{-1}$, $R = 25$ nm, and $b = 2.5$ nm ($\theta_c = 2.9°$) for the radius of the zone in which lipids mix.

This estimated mean capture time scale is comparable to the fastest values of $t_{R18\ rise}$ observed (Fig. S8). The result scales as R^2/D, suggesting that variability in R and perhaps D may cause some of the observed spread in observed values of $t_{R18\ rise}$ (Fig. S8). There is a correlation between the time scale of lipid mixing (as measured by $t_{R18\ rise}$) and the type of event (Fig. S8). For prompt, full fusion events, $t_{R18\ rise}$ is almost always <15 ms, suggesting little or no barrier or bottleneck to lipid mixing once fusion begins.

For hemifusion events (both productive and dead-end), $t_{R18\ rise}$ is usually in the time 15–120 ms, much longer than the diffusion-limited estimates. The longer values are probably determined by the rate of flip-flop and dequenching of inner leaflet labels after hemifusion but prior to core fusion. If so, then the apparent R18 dequenching time scale, ~60 ms, is several times faster than the flip-flop time scale of ~200 ms inferred from relief of calcein → R18 FRET (Results). This is sensible. Self-quenching of R18 can be completely relieved when only a fraction of the inner-leaflet R18 molecules have flip-flopped out, whereas FRET continues until all inner-leaflet labels are gone. As further confirmation of R18 flip-flop, we plotted analogous t_{rise} distributions using TRITC-DHPE as the lipid label (data not shown). The distributions are narrow, like that of Fig. S8 a, for prompt, full fusion, for productive hemifusion, and for dead-end hemifusion events.

Table S1. Branching fractions into hemifusion events using different lipid markers with and without calcein content labeling. In each case, the v-SNARE vesicle contained 60% DOPE, 15% DOPS, the lipid marker as shown, and the remainder POPC. Data obtained from 40 ms/frame movies by analysis of lipid marker behavior only.

Lipid marker	**Calcein (mM)**	**Laser(s) On**	N_{total}[a]	**Lipid-based Branching Fractions**[b]			
				f_{fus}	f_{hemi}	f_{core}	$f_{dead\text{-}end}$
1% TRITC-DHPE	0	514 nm	112	0.66	0.34	0.14	0.20
5% R18	0	561 nm	133	0.96	0.036	0.014	0.022
5% Texas Red-DHPE	0	561 nm	100	0.83	0.17	0.08	0.09
5% Texas Red-DHPE	50	561 nm	67	0.85	0.15	0.06	0.09
5% Texas Red-DHPE	50	561 nm + 488 nm	44	0.86	0.14	0.07	0.07

[a] Total number of events analyzed.

[b] Branching fractions based on lipid marker behavior only. Hemifusion was recorded only when a second outgoing wave or a bright core persistent after the first wave was observed. As described in the main text, this method misses many fast hemifusion events, i.e., the data in this table should not match the data in Table 1. Branching fractions defined so that $f_{fus} + f_{hemi} = 1$ and $f_{hemi} = f_{core} + f_{dead\text{-}end}$.

Supplementary References

S1. Liu, T.T., W.C. Tucker, A. Bhalla, E.R. Chapman, and J.C. Weisshaar. 2005. SNARE-driven, 25-millisecond vesicle fusion *in vitro*. *Biophys. J.* 89(4):2458-2472.

S2. Weinstein, J.N., S. Yoshikami, P. Henkart, R. Blumenthal, and W.A. Hagins. 1977. Liposome-Cell Interaction - Transfer and Intracellular Release of a Trapped Fluorescent Marker. *Science* **195**(4277):489-492.

S3. Axelrod, D. 2001. Selective imaging of surface fluorescence with very high aperture microscope objectives. *Journal of Biomedical Optics* **6**(1):6-13.

S4. Liu, T., T. Wang, E.R. Chapman, and J.C. Weisshaar. 2008. Productive hemifusion intermediates in fast vesicle fusion driven by neuronal SNAREs. *Biophys. J.* 94(4):1303-1314.

S5. Bowen, M.E., K. Weninger, A.T. Brunger, and S. Chu. 2004. Single molecule observation of liposome-bilayer fusion thermally induced by soluble N-ethyl maleimide sensitive-factor attachment protein receptors (SNAREs). *Biophys. J.* 87(5):3569-3584.

S6. Lakowicz, J.R. 1999. Principles of Fluorescence Spectroscopy. New York: Kluwer Academic/Plenum.

S7. Chernomordik, L., A. Chanturiya, J. Green, and J. Zimmerberg. 1995. The Hemifusion Intermediate and Its Conversion to Complete Fusion - Regulation by Membrane-Composition. *Biophys. J.* 69(3):922-929.

S8. Berg, H.C., and E.M. Purcell. 1977. Physics of chemoreception. *Biophys. J.* 20(2):193-219.

S9. Linderman, J.J., and D.A. Lauffenburger. 1986. Analysis of intracellular receptor/ligand sorting. Calculation of mean surface and bulk diffusion times within a sphere. *Biophys. J.* 50(2):295-305.

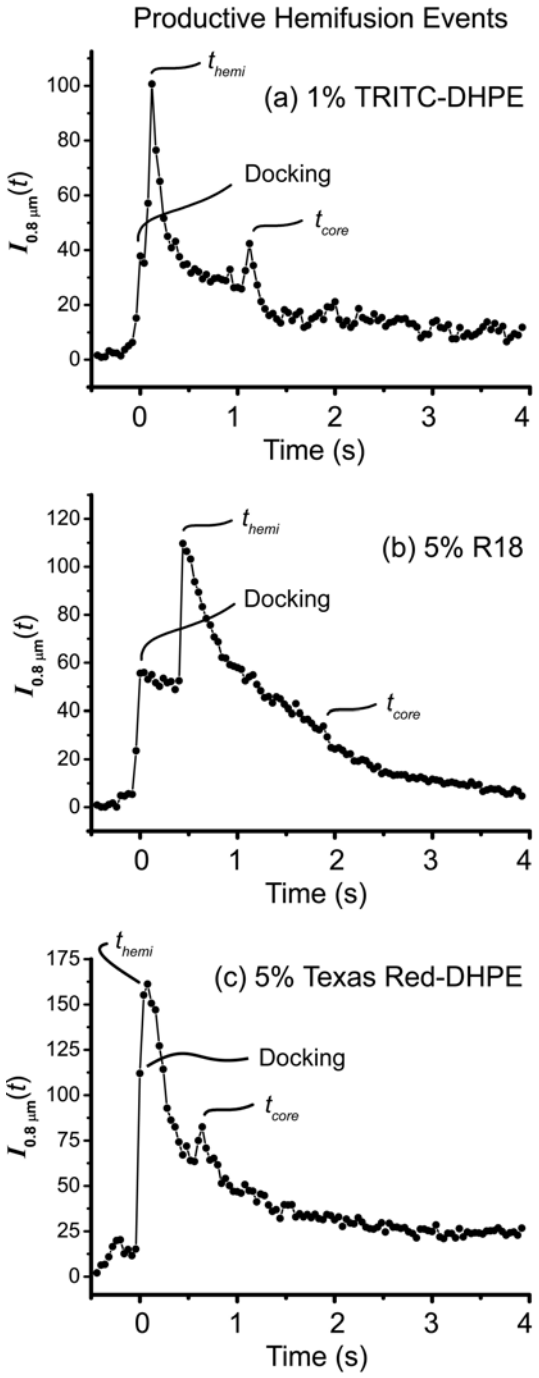

Figure S1. Representative examples of fluorescence intensity traces $I_{0.8\,\mu m}(t)$ (intensity integrated over a 0.8 μm radius circle) for productive hemifusion events from 40 ms/frame, one-color movies. Lipid markers within the v-SNARE vesicles were **(a)** 1% TRITC-DHPE, **(b)** 5% R18, and **(c)** 5% Texas Red-DHPE. The v-SNARE vesicles contain 60% DOPE. Laser intensity is 30 μW in an 800 μm^2 area.

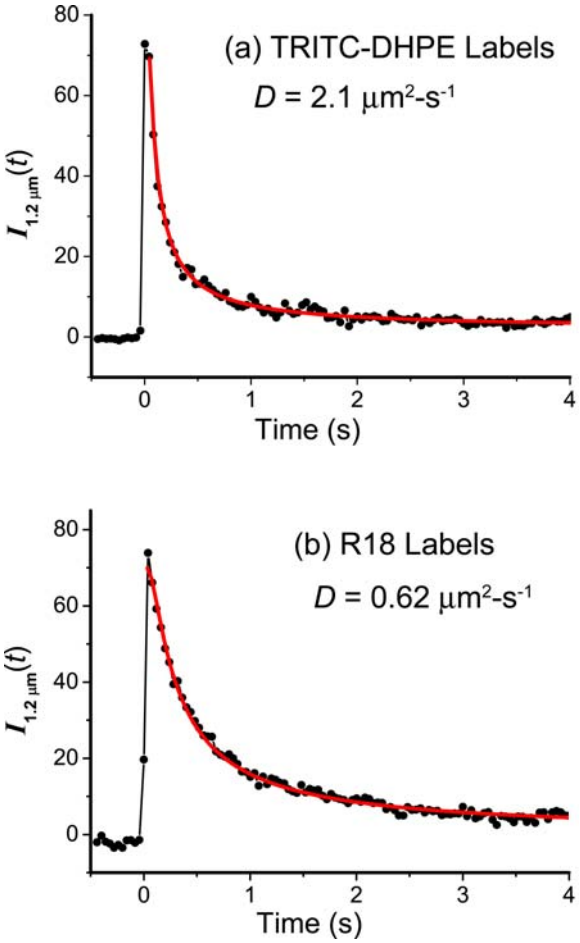

Figure S2. Fluorescence intensity traces $I_{0.8\mu m}(t)$ (intensity integrated over a 0.8 μm radius circle) for two well isolated, prompt, full fusion events (Type 1). The v-SNARE vesicles were labeled with **(a)** 1%TRITC-DHPE, and **(b)** 5% R18. Solid red lines are least squares fits of the data to the two-dimensional diffusion equation, with best-fit diffusion coefficients as shown. See Ref. 38 for details.

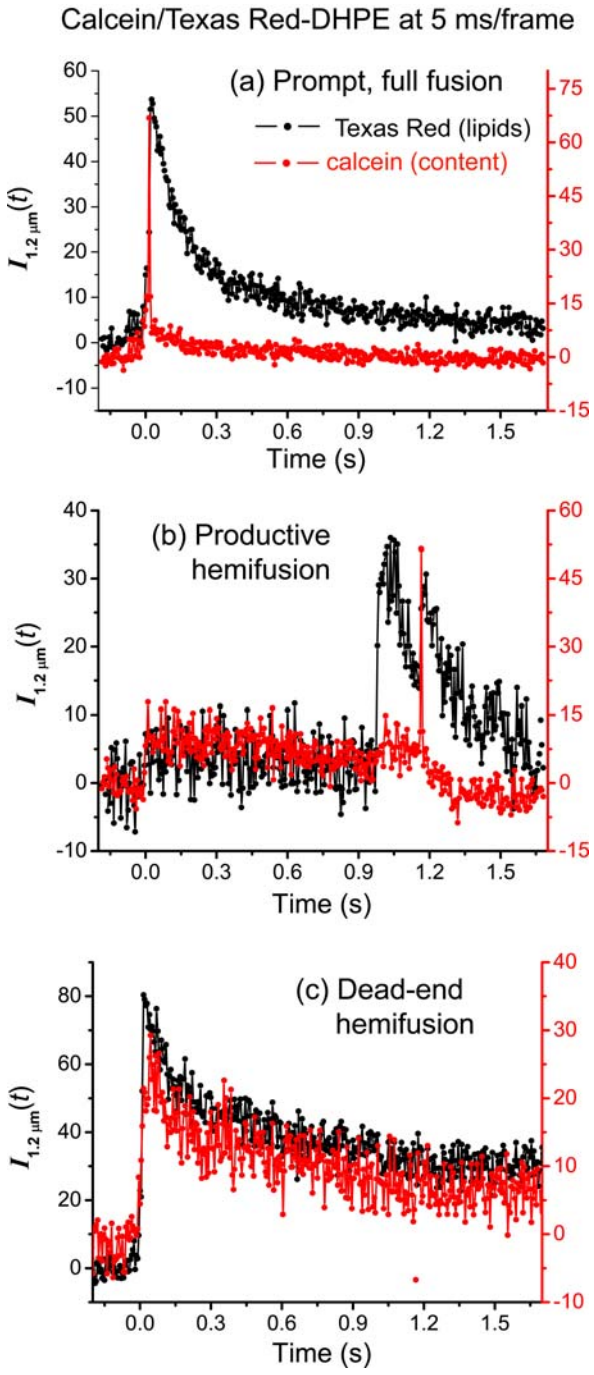

Figure S3. Examples of the fluorescence intensity $I_{1.2\mu m}(t)$ (intensity integrated over a 1.2 μm radius circle) from two-color, 5-ms movies using v-SNARE vesicles labeled with 5% Texas Red-DHPE and 50 mM calcein content. **(a)** Prompt, full fusion (Type 1). **(b)** Productive hemifusion (Type 2). **(c)** Dead-end hemifusion (Type 3). The v-SNARE vesicle lipid composition is 20% POPC, 15% DOPS, 60% DOPE, and 5% Texas Red-DHPE in all cases.

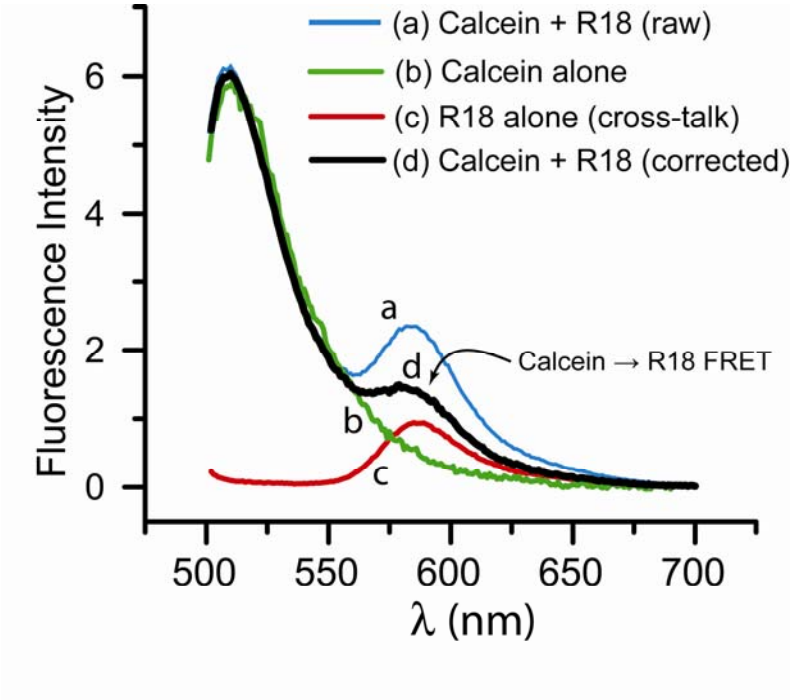

Figure S4. Direct evidence of FRET from calcein content to R18 lipid labels in protein-free vesicles. Emission spectra obtained in a standard fluorimeter with excitation at 488 nm or at 561 nm. **(a)** Solution of vesicles containing 50 mM calcein and 5% R18, showing both calcein (560 nm) and rhodamine (510 nm) emission peaks. **(b)** Solution of vesicles containing 50 mM calcein without R18 labels showing only the calcein emission. **(c)** Solution of vesicles containing only the R18 labels without calcein. The emission is due to "cross-talk", weak excitation of R18 at 488 nm. **(d)** Spectrum of (a) with contribution of rhodamine cross-talk subtracted out. The remainder spectrum shows clear evidence of FRET. For the subtraction, the solutions of part (a) and of part (c) were both excited at the rhodamine excitation wavelength of 561 nm. The resulting rhodamine emission intensities of (c) was scaled to correct for possible differences in vesicle concentrations prior to subtraction. There is only negligible excitation of calcein at 561 nm (negligible "reverse cross-talk"; data not shown).

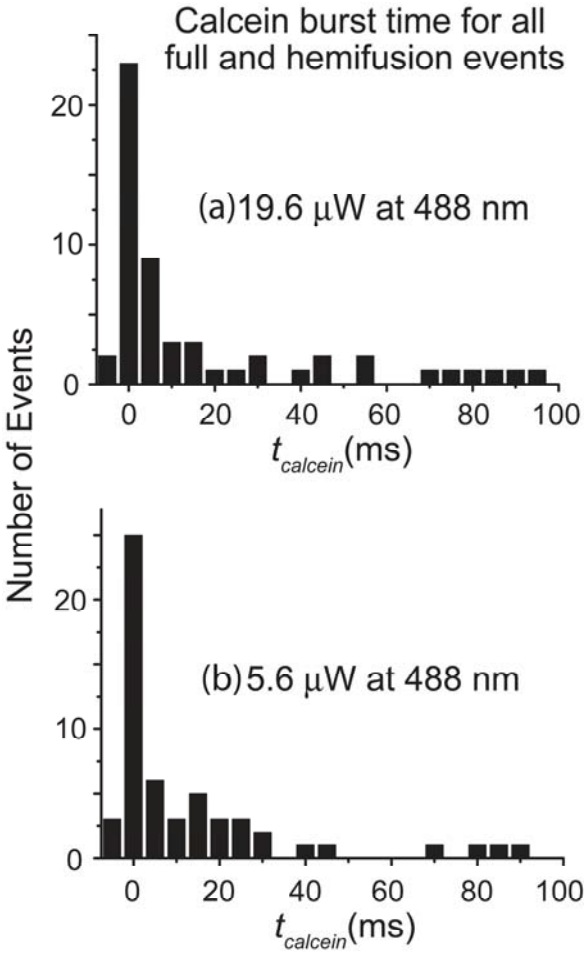

Figure S5. Test for possible effects of laser intensity on fusion kinetics in 5-ms, two-color movies using 5% R18 and 50 mM calcein as labels. Histograms of the time between the onset of lipid diffusion and content release, including all full fusion and productive hemifusion events. **(a)** 5 μW at 561 nm and 19.6 μW at 488 nm illuminating a ~160 μm^2 area. **(b)** 5 μW at 561 nm and 5.6 μW at 488 nm for the same area. The v-SNARE vesicle lipid composition is 20% POPC, 15% DOPS, 60% DOPE and 5%

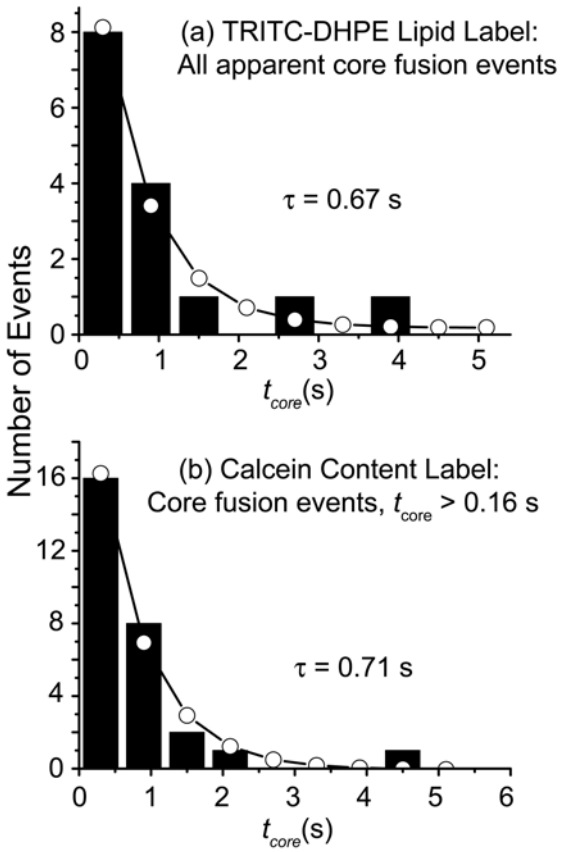

Figure S6. Comparison of apparent distribution of core fusion events for 60% DOPE v-SNARE vesicles as detected by **(a)** the second burst of dequenching of TRITC-DHPE labels (or the decay of a visible core of TRITC fluorescence following an initial burst) and by **(b)** the narrow calcein burst in vesicles labeled with 5% R18 and 50 mM calcein. For the sake of comparison, (b) includes only those calcein events occurring at least 160 ms after hemifusion. In (a), events faster than 160 ms are presumably obscured by residual fluorescence from the first outgoing wave of TRITC-DHPE lipids. The similarity of the histograms indicates that the core kinetics are essentially the same in both labeling schemes. In both cases, open circles show the best fit by a single exponential decay.

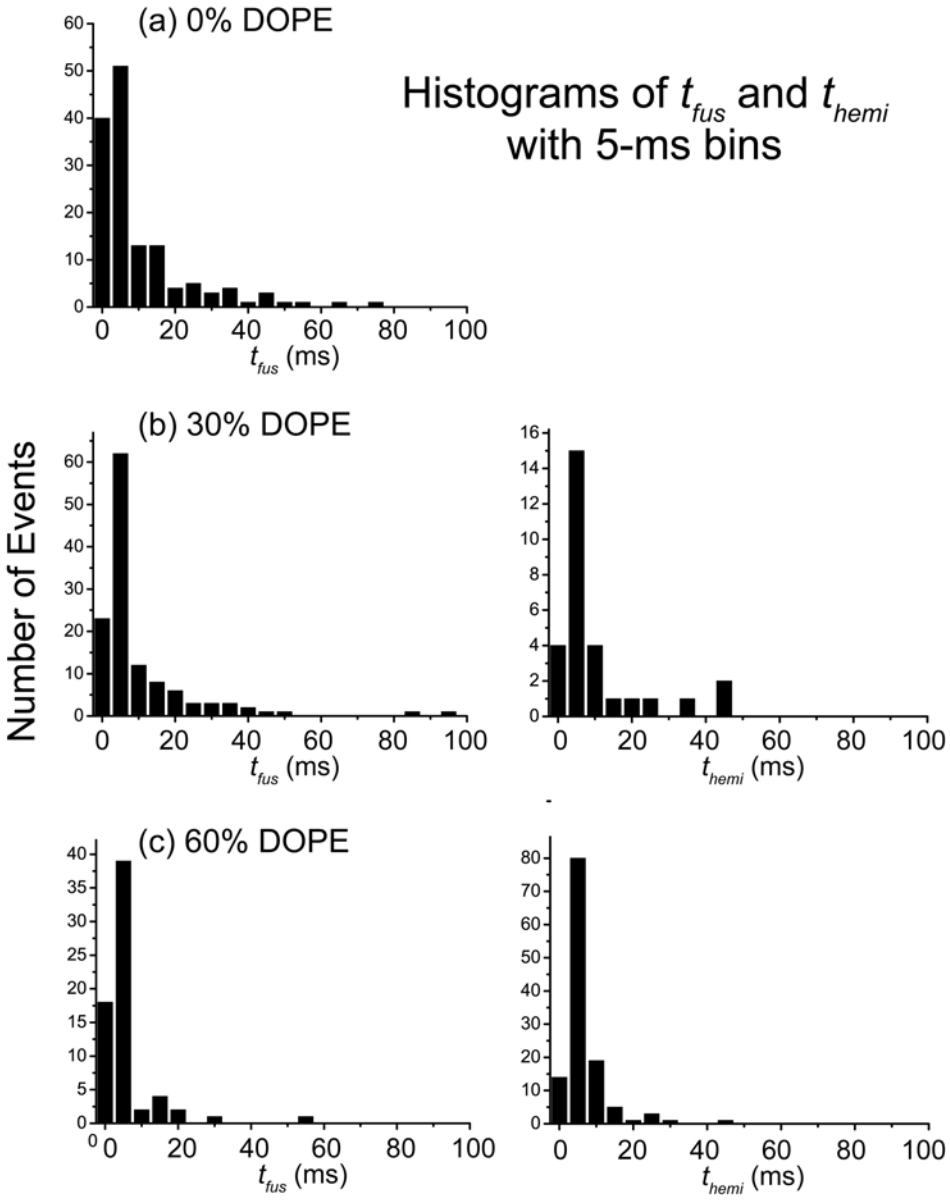

Figure S7. Histograms of t_{fus} and t_{hemi} for v-SNARE vesicles with **(a)** no DOPE, **(b)** 30% DOPE, and **(c)** 60% DOPE from two-color, 5 ms/frame movies. This is the same data as in Fig. 4 of the main text, but binned into 5-ms intervals, the actual time resolution of the movies. The distributions are choppy at early times due to statistics and also due to the variable phase of the camera frames relative to actual events.

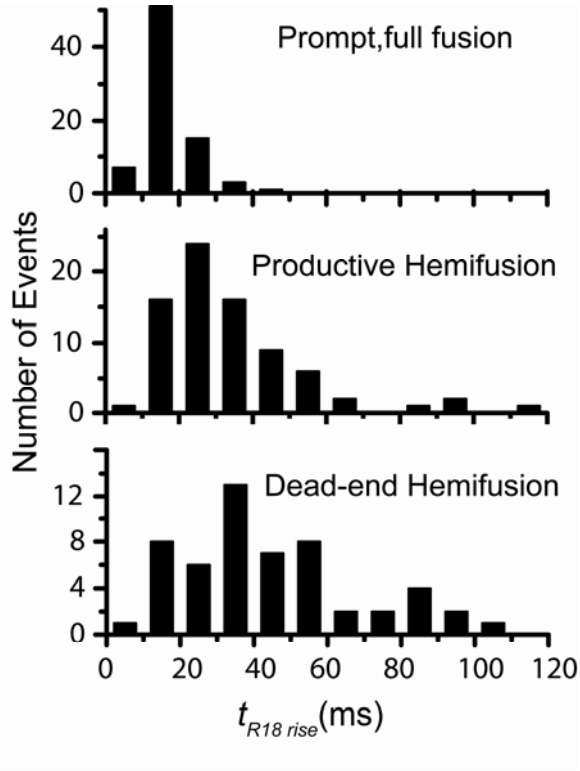

Figure S8. Histograms of the risetime of the R18 dequenching signal classified for the three different types of fusion outcome as shown. 60% DOPE in the v-SNARE vesicles. Larger values of $t_{R18\ rise}$ correlate with productive or dead-end hemifusion.